JACS
JOURNAL OF THE AMERICAN CHEMICAL SOCIETY
Communication
pubs.acs.org/JACS

Monodisperse Au Nanoparticles for Selective Electrocatalytic Reduction of CO_2 to CO

Wenlei Zhu,[†] Ronald Michalsky,[‡] Önder Metin,[†,§] Haifeng Lv,[†] Shaojun Guo,[†] Christopher J. Wright,[†] Xiaolian Sun,[†] Andrew A. Peterson,*[,‡] and Shouheng Sun*[,†]

[†]Department of Chemistry and [‡]School of Engineering, Brown University, Providence, Rhode Island 02912, United States
[§]Department of Chemistry, Faculty of Science, Atatürk University, 25240 Erzurum, Turkey

Supporting Information

ABSTRACT: We report selective electrocatalytic reduction of carbon dioxide to carbon monoxide on gold nanoparticles (NPs) in 0.5 M $KHCO_3$ at 25 °C. Among monodisperse 4, 6, 8, and 10 nm NPs tested, the 8 nm Au NPs show the maximum Faradaic efficiency (FE) (up to 90% at −0.67 V vs reversible hydrogen electrode, RHE). Density functional theory calculations suggest that more edge sites (active for CO evolution) than corner sites (active for the competitive H_2 evolution reaction) on the Au NP surface facilitates the stabilization of the reduction intermediates, such as COOH*, and the formation of CO. This mechanism is further supported by the fact that Au NPs embedded in a matrix of butyl-3-methylimidazolium hexafluorophosphate for more efficient COOH* stabilization exhibit even higher reaction activity (3 A/g mass activity) and selectivity (97% FE) at −0.52 V (vs RHE). The work demonstrates the great potentials of using monodisperse Au NPs to optimize the available reaction intermediate binding sites for efficient and selective electrocatalytic reduction of CO_2 to CO.

The ever-increasing worldwide consumption of fossil fuels has accelerated the depletion of these finite natural resources and led to overproduction of the greenhouse gas carbon dioxide.[1] To meet the fuel and chemical demands in a sustainable way, the overly produced CO_2 must be converted into reusable carbon forms.[2] Among many different approaches developed thus far for CO_2 reactivation, electrochemical reduction of CO_2 is considered a potentially "clean" method as the reduction proceeds at the expense of a sustainable supply of electric energy.[3] Theoretically, CO_2 can be reduced in an aqueous solution (pH 7, 1 M electrolyte at 25 °C and 1 atm CO_2) to form carbon monoxide, formic acid, methane or other hydrocarbons at potentials around +0.2 to −0.2 V (vs reversible hydrogen electrode (RHE); all potentials reported in this paper are with respect to RHE).[4] Experimentally, however, very negative potentials must be applied to initiate CO_2 reduction.[4] These large overpotentials not only consume more electrical energy but also promote the uncontrolled formation of competitive reduction products, such as H_2, causing low energetic efficiencies and poor selectivity.[5,6]

To succeed in CO_2 reduction and conversion, highly efficient catalysts must be developed to lower the CO_2 reduction overpotentials and to control the energy pathways of reaction intermediates. Various metal electrocatalysts have been screened experimentally[7−12] and analyzed computationally[13−15] to rationalize their activity and selectivity for CO_2 reduction. Recent advances in the synthesis of nanoparticles (NPs) allow for testing of potentially increased reaction kinetics due to the controlled surface area and surface morphology achieved. This is demonstrated by electrochemical reduction of CO_2 into hydrocarbons on Cu NPs,[16,17] or into CO on gold-based NPs/clusters.[18−20] Recently, a new form of Au nanostructured catalyst made by anodization and electroreduction of an Au electrode was demonstrated to show high selectivity for catalyzing CO_2 reduction to CO: its Faradaic efficiency (FE) was ∼96% at −0.35 V with current densities between 2 and 4 mA/cm^2.[18] It is suggested that the increased stabilization of a reduced CO_2 adsorbate or the adsorbed reaction intermediate COOH as well as the weakened CO binding on the Au surface contribute to this selective reduction of CO_2 to CO.[18,20] However, the structure feature of the catalyst surface is difficult to characterize, which complicates further catalyst optimization.

Considering the size effect commonly observed in NPs and the promising results demonstrated from nanostructured Au, we chose to study monodisperse Au NPs as catalysts for electrochemical reduction of CO_2 in 0.5 M $KHCO_3$ (pH 7.3) at room temperature. We screened 4, 6, 8, and 10 nm Au NPs and found that the 8 nm Au NPs were especially active for CO_2 reduction into CO. Using density functional theory (DFT) calculations, we rationalized this enhanced activity and selectivity with the presence of dominant edge sites on the 8 nm NP surface, which facilitates the adsorption/stabilization of key reaction intermediates (such as COOH*) for the CO_2 reduction into CO and inhibits the hydrogen evolution reaction (HER). This reaction model was further supported experimentally as Au NPs embedded in a matrix of butyl-3-methylimidazolium hexafluorophosphate (BMIM-PF_6), a more efficient COOH* stabilizer, were indeed more active and selective for CO_2 reduction into CO. The composite catalyst containing 8 nm NPs exhibited up to 97% FE toward CO and a mass activity of 3 A/g at −0.52 V. Our work demonstrates the great potential of tuning electrocatalysis of Au NPs by creating optimal edge sides on their surface for effective CO_2 reduction into CO.

Received: September 12, 2013
Published: October 24, 2013

   dx.doi.org/10.1021/ja409445p | J. Am. Chem. Soc. 2013, 135, 16833−16836

The monodisperse Au NPs were prepared by procedures modified from previous publications (see Supporting Information (SI)).[21−23] Transmission electron microscopy (TEM) images show the diameters of the polyhedral Au NPs to be 7.7 ± 0.3 nm (Figure 1a) and 4.1 ± 0.3, 6.3 ± 0.3, and 10.5 ± 0.5

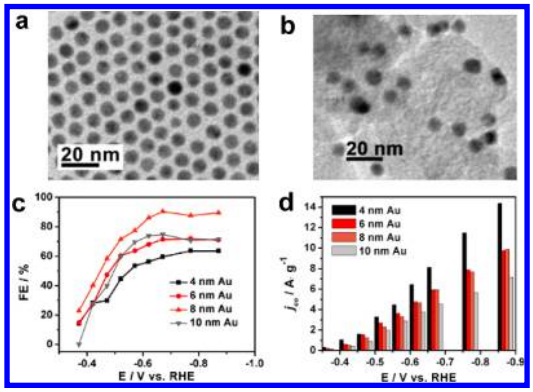

Figure 1. TEM images of (a) the 8 nm Au NPs and (b) the C-Au NPs. (c) Potential-dependent FEs of the C-Au on electrocatalytic reduction of CO_2 to CO. (d) Current densities for CO formation (mass activities) on the C-Au at various potentials.

nm (Figure S1a−c). X-ray diffraction (XRD) patterns of the Au NPs are shown in Figure S2. Using Scherrer's formula, we analyzed the line broadening of the 4, 6, 8, and 10 nm Au(111) peaks and estimated the crystallite diameters of the NPs to be 2.0, 2.3, 4.0, and 5.9 nm, respectively, which are all smaller than the particle diameters estimated from TEM analysis, indicating a polycrystalline nature of the Au NPs.[21] The Au NPs were deposited on carbon support (Ketjen EC300J) (at a weight ratio of 1:1) and annealed in air for 8 h at 165 °C to remove the surfactant as reported,[24,25] giving C-Au. TEM analyses of the C-Au showed no NP morphological changes or aggregation after the treatment (Figure 1b). Actual Au weight ratios in the C-Au catalysts were measured by inductively coupled plasma atomic emission spectroscopy (ICP-AES) to be 0.21, 0.28, 0.32, 0.35 g Au per gram of C-Au for the 4, 6, 8, and 10 nm Au NPs, respectively.

To study electrocatalytic reduction of CO_2 on the C-Au catalyst, a C-Au paste containing 20 mg of C-Au NPs, 3 mg of polyvinylidene fluoride (PVDF) and a few drops of *N*-methyl-2-pyrrolidone (NMP) was prepared (see SI). The paste was then painted onto a carbon paper (Toray TGP-H-060)[26,27] and dried under vacuum to serve as a working electrode. The electrocatalysis was performed in a conventional H-cell (separated by Nafion 212) with 0.5 M $KHCO_3$ solution (pH 7.3). In the reported conditions, CO and H_2 were the only two detectable reaction products with net total FE at 100.6% ± 3.9%. Carbon support was found to be stable and produced only low amounts of H_2 (see Figure S3). Figure 1c shows the potential-dependent FEs of different C-Au NPs for CO formation. Significant amounts of CO are generated at an onset potential of −0.37 V, which is 0.26 V below the theoretical equilibrium potential (−0.11 V). FE increases when more negative potentials are applied and reaches near saturation at −0.65 V. The CO_2 reduction activity is size-dependent and the 8 nm NPs are the most active for CO formation with FE reaching 90% at −0.67 V, which is better than other reported polycrystalline Au catalysts (87% FE at −0.74 V).[16] Figure 1d summarizes the mass activities of Au NPs at various potentials for CO formation. The 4 nm Au NPs have the highest value due to their small size and large surface area.

Electrochemical reduction of CO_2 to CO in an aqueous solution depends on the energetic stabilization of reduction intermediates by catalytically active surfaces.[13,14,28] The reaction is suggested[14,28] to include the following steps:

$$CO_2 + H^+(aq) + e^- + * \rightarrow COOH* \quad (1)$$

$$COOH* + H^+(aq) + e^- \rightarrow CO* + H_2O \quad (2)$$

$$CO* \rightarrow CO + * \quad (3)$$

$$H^+(aq) + e^- + * \rightarrow H* \quad (4)$$

$$H* + H^+(aq) + e^- \rightarrow H_2 + *$$

or

$$H* + H* \rightarrow H_2 + 2* \quad (5)$$

where the asterisk denotes either a surface-bound species or a vacant catalytically active site. The formation of CO does not only depend on the stabilization (step 1) and reduction (step 2) of a COOH*, but also on the ability of the catalyst to liberate the CO product (step 3). For high CO selectivity, the catalyst needs to balance steps 1−3 while inhibiting the hydrogen evolution reaction (HER) via H^+ reduction (steps 4 and 5), a major side reaction that is often observed in studying electrochemical reduction of CO_2.

To understand the origin of the high CO selectivity on Au NPs, we applied DFT to calculate the free energies of these five elementary reaction steps. The catalyst was modeled in a number of different geometries with the Grid-based projector-augmented wave (GPAW) electronic-structure code in order to understand the reactivity of different Au features (see SI). The total energy of these surfaces or clusters with or without adsorbates was calculated and converted to free energy (ΔG) at 25 °C, 1 atm, and −0.11 V, the theoretical equilibrium potential of CO_2 reduction into CO. Figure 2a shows the calculated free energy diagram for CO_2 reduction on Au(111), Au(211), and Au_{13}, based on the computational hydrogen electrode model.[34] The literature data shown for comparison (dots and the related bar as the arithmetic average) are taken from Au(111),[29−33] Au(211),[13,28,29,32] and Au_{13}[29] or Au_{12}[32] and are converted to

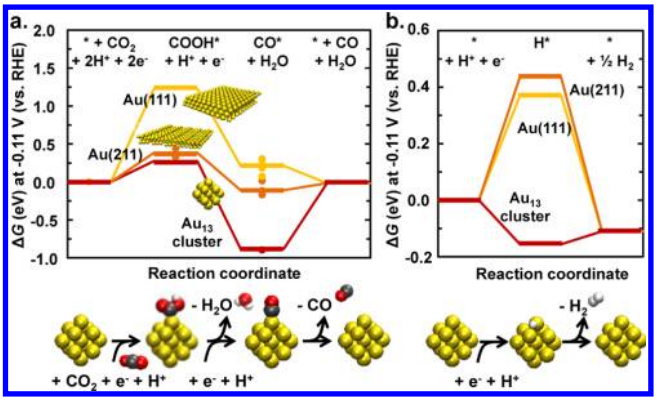

Figure 2. Free energy diagrams for electrochemical reduction of (a) CO_2 to CO and (b) protons to hydrogen on Au(111) (yellow symbols), Au(211) (orange symbols), or a 13-atom Au cluster (red symbols) at −0.11 V. Horizontal lines are calculations from this study, and dots are the literature data[13,28−33] converted to free energies.

dx.doi.org/10.1021/ja409445p | J. Am. Chem. Soc. 2013, 135, 16833−16836

the same reference energies. All energies are plotted at the reversible potential of the CO_2 to CO reaction and a "perfect" catalyst would exhibit zero free energy change throughout the reaction. On Au(111) at −0.11 V, CO_2 activation through COOH* formation is associated with a high increase in free energy, ΔG. This energy can be supplied in the form of the overpotential required to form reaction intermediates. On Au(211), the required ΔG to form the COOH* intermediate is significantly lower, compared to Au(111), suggesting a higher activity of stepped surfaces in CO_2 reduction. On Au_{13}, COOH* formation is slightly more facile than on Au(211); however, the Au_{13} tends to overbind CO, relative to Au(211), which would be expected to decrease the rate of product liberation. It should be noted that the effect of adsorbate coverage (1/4 to 1/16 of a monolayer) does not alter the relative positions of the free energy levels significantly.[13,28−33]

The calculated ΔG diagram suggests that the overpotential of CO_2 reduction or the partial current of CO formation on Au NPs at a given potential can be controlled by the density of catalytically active edges, which is controllable by NP size and surface structure. Similar trends can be seen with the calculated ΔG changes of adsorbed hydrogen on Au(111), Au(211), and the Au_{13} cluster (Figure 2b). Au surfaces tend to be poor for HER due to the metal's nobility.[35] However, the increased affinity of low-coordination sites for H, exhibited by the Au_{13} cluster, turns Au into a much more optimal HER catalyst. The ΔG of H* on the Au_{13} cluster is below the ΔG of COOH*, suggesting formation of H_2 at low potentials on low-coordination sites. The Au(211) facet, on the other hand, is expected to yield high CO selectivity due to weak binding of H* relative to COOH* on this facet. Edge sites favor CO formation while corner sites are active for H_2 evolution.

To address size-dependent electrocatalytic properties of the Au NPs, we treated the NPs as perfect cuboctahedra and obtained the relationship between the density of catalytically active surface sites and the cluster diameter (Figure 3). At a diameter of about 2.7 nm, the fraction of the active surface atoms equals the fraction of bulk atoms, suggesting that smaller particles will have higher mass activities. NPs below this size may additionally be expected to show finite size effects.[29,36,37]

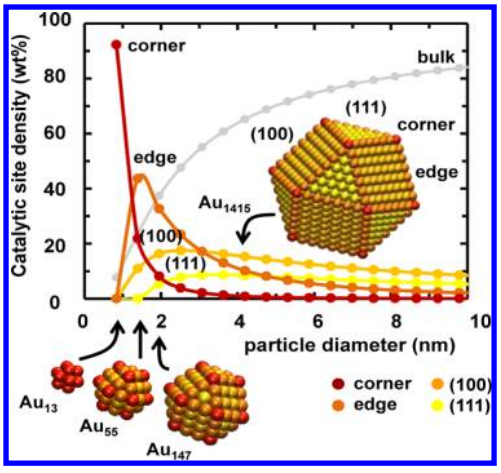

Figure 3. Density of adsorption sites (yellow, light orange, dark orange, or red symbols for (111), (001), edge, or corner on-top sites, respectively) on closed-shell cuboctahedral Au clusters vs the cluster diameter. The weight fraction of Au bulk atoms is marked with gray dots.

NPs with diameters ∼4 nm maintain a relatively high density of edge sites between 10 and 13%; at larger particle diameters, NP catalysis may be dominated by the close-packed (111) facets, leading to the reduced selectivity for CO over H_2 (Figure 2). Smaller particles have a higher density of strongly binding corner sites, which are active for H_2 evolution. Our data on FE for CO formation (Figure 1c) suggest that the origin of the activity of the Au NPs lies not in a particular quantum size effect but in an optimal density of catalytically active edge sites. The 8 nm Au NPs with 4 nm crystallite diameter appear to provide a near-optimum number of edge sites that are particularly active for CO_2 reduction into CO while minimizing the number of corner sites active for the HER.

The ΔG diagram of the CO_2 reduction into CO shows that the major fraction of the overpotential comes from the need to energetically stabilize COOH* (Figure 2). A recent report suggests that ionic liquids (ILs) may lower the overpotential for CO evolution,[38] which we hypothesize may be due to the stabilization of the adsorbed COOH* intermediate. This indicates that combining C-Au NPs with IL (C-Au-IL) may allow for highly selective and active CO_2 reduction into CO. To test this hypothesis, we prepared C-Au-IL by adding IL ($BMIM\text{-}PF_6$) to previous C-Au-PVDF paste and painted it onto carbon paper. The IL effect on CO_2 reduction was further studied by mixing 20 mg of the C-Au (8 nm) with different volumes of IL. Figure S4 shows the FEs and mass activities for CO formation in the presence of 5, 10, 15, or 20 μL of IL. The addition of IL increases the FE significantly in the low potential region. In the region more negative than −0.6 V, both FEs and mass activities decrease sharply with increased IL loadings. This is likely caused by the stronger adsorption of hydrophobic IL, which reduces the active sites and inhibits protonation of the reduced CO_2. For 20 mg of the C-Au, 10 μL of IL is the optimum amount that can be used to enhance Au catalysis. Figures 4a,b and S5 show the activity of the C-Au-IL (10 μL of

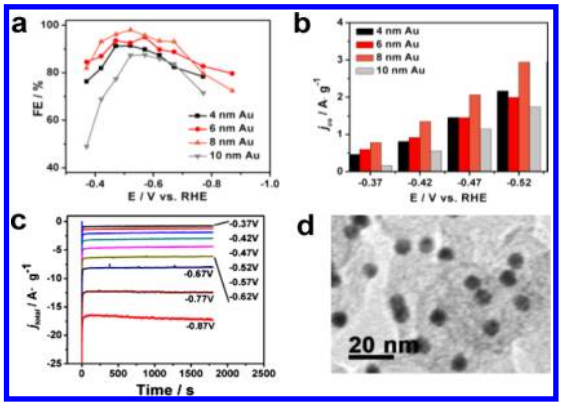

Figure 4. Potential-dependent (a) FEs and (b) mass activities of the C-Au-IL on electrocatalytic reduction of CO_2 to CO in the presence of 10 μL IL. (c) Plot of mass current densities over time of the C-Au-IL (8 nm NPs, 10 μL IL) for CO_2 reduction. (d) TEM image of the 8 nm NPs in C-Au-IL after CO_2 reduction reaction study.

IL) for reduction of CO_2 to CO. Comparing to the FE and mass activities of the C-Au NPs (Figure 1c,d), we can see that in the presence of 10 μL of IL, the same 8 nm Au NPs show much higher selectivity (∼80% FE at −0.37 V and 97% FE at −0.52 V) and highest mass activities for CO formation at all potential ranges. Both C-Au and C-Au-IL retain their catalytic activities in a wide potential region (Figures S6 and 4c), and the

dx.doi.org/10.1021/ja409445p | J. Am. Chem. Soc. 2013, 135, 16833−16836

Au NPs in the C-Au-IL show no morphological change after CO_2 reduction (Figure 4d), indicating the C-Au NPs are stable in the current electrochemical reaction condition.

In summary, we have synthesized a series of monodisperse Au NPs and studied their electrocatalytic reduction of CO_2 to CO. Among 4, 6, 8, and 10 nm Au NPs tested, the 8 nm Au NPs show the highest selectivity with their FE reaching 90% at −0.67 V. DFT calculations suggest that the highly selective CO formation on the 8 nm Au NPs is due to presence of an optimum ratio of the edge sites, which are active for CO_2 reduction, over corner sites, which are active for H_2 evolution. When embedded in a matrix of butyl-3-methylimidazolium hexafluorophosphate, the Au NPs become even more active for CO_2 reduction. The composite catalyst containing 8 nm Au NPs has FE up to 97% and mass activity of about 3 A/g at −0.52 V. Our study provides evidence that stabilization of COOH* is key to the CO_2 reduction activity enhancement, and demonstrates great potentials of monodisperse Au NPs for the selective electrochemical reduction of CO_2 to CO. With the recent advances in chemical syntheses of monodisperse NPs and computational methodology, various NP catalysts can now be designed and tested, making it possible to control specific reaction pathways and to achieve selective electrochemical reactivation of CO_2 into a desired form of carbon.

■ ASSOCIATED CONTENT

Supporting Information

Experimental methods, analyses of Au NPs and their electrocatalysis, and computational details. This material is available free of charge via the Internet at http://pubs.acs.org.

■ AUTHOR INFORMATION

Corresponding Authors

andrew_peterson@brown.edu
ssun@brown.edu

Notes

The authors declare no competing financial interest.

■ ACKNOWLEDGMENTS

This material is based upon work supported by the National Science Foundation under the Center for Chemical Innovation "CO_2 as a Sustainable Feedstock for Chemical Commodities", CHE-1240020. High-performance computational resources were employed at the Center for Computation and Visualization, Brown University.

■ REFERENCES

(1) Goeppert, A.; Czaun, M.; May, R. B.; Prakash, G. K. S.; Olah, G. A.; Narayanan, S. R. *J. Am. Chem. Soc.* **2011**, *133*, 20164.
(2) Graves, C.; Ebbesen, S. D.; Mogensen, M.; Lackner, K. S. *Renewable Sustainable Energy Rev.* **2011**, *15*, 1.
(3) Whipple, D. T.; Kenis, P. J. A. *J. Phys. Chem. Lett.* **2010**, *1*, 3451.
(4) Benson, E. E.; Kubiak, C. P.; Sathrum, A. J.; Smieja, J. M. *Chem. Soc. Rev.* **2009**, *38*, 89.
(5) Costentin, C.; Robert, M.; Saveant, J. M. *Chem. Soc. Rev.* **2013**, *42*, 2423.
(6) Gattrell, M.; Gupta, N.; Co, A. *J. Electroanal. Chem.* **2006**, *594*, 1.
(7) De Jesus-Cardona, H.; del Moral, C.; Cabrera, C. R. *J. Electroanal. Chem.* **2001**, *513*, 45.
(8) Innocent, B.; Liaigre, D.; Pasquier, D.; Ropital, F.; Leger, J. M.; Kokoh, K. B. *J. Appl. Electrochem.* **2009**, *39*, 227.
(9) Chen, Y. H.; Kanan, M. W. *J. Am. Chem. Soc.* **2012**, *134*, 1986.
(10) Jitaru, M.; Lowy, D. A.; Toma, M.; Toma, B. C.; Oniciu, L. *J. Appl. Electrochem.* **1997**, *27*, 875.
(11) Noda, H.; Ikeda, S.; Oda, Y.; Imai, K.; Maeda, M.; Ito, K. *Bull. Chem. Soc. Jpn.* **1990**, *63*, 2459.
(12) Hori, Y.; Murata, A.; Kikuchi, K.; Suzuki, S. *J. Chem. Soc., Chem. Commun.* **1987**, 728.
(13) Peterson, A. A.; Nørskov, J. K. *J. Phys. Chem. Lett.* **2012**, *3*, 251.
(14) Peterson, A. A.; Abild-Pedersen, F.; Studt, F.; Rossmeisl, J.; Nørskov, J. K. *Energy Environ. Sci.* **2010**, *3*, 1311.
(15) Durand, W. J.; Peterson, A. A.; Studt, F.; Abild-Pedersen, F.; Nørskov, J. K. *Surf. Sci.* **2011**, *605*, 1354.
(16) Tang, W.; Peterson, A. A.; Varela, A. S.; Jovanov, Z. P.; Bech, L.; Durand, W. J.; Dahl, S.; Nørskov, J. K.; Chorkendorff, I. *Phys. Chem. Chem. Phys.* **2012**, *14*, 76.
(17) Yang, N. J.; Gao, F.; Nebel, C. E. *Anal. Chem.* **2013**, *85*, 5764.
(18) Chen, Y. H.; Li, C. W.; Kanan, M. W. *J. Am. Chem. Soc.* **2012**, *134*, 19969.
(19) Xu, Z. C.; Lai, E. C.; Yang, S. H.; Hamad-Schifferli, K. *Chem. Commun.* **2012**, *48*, 5626.
(20) Kauffman, D. R.; Alfonso, D.; Matranga, C.; Qian, H. F.; Jin, R. C. *J. Am. Chem. Soc.* **2012**, *134*, 10237.
(21) Lee, Y.; Loew, A.; Sun, S. H. *Chem. Mater.* **2010**, *22*, 755.
(22) Peng, S.; Lee, Y. M.; Wang, C.; Yin, H. F.; Dai, S.; Sun, S. H. *Nano Res.* **2008**, *1*, 229.
(23) Lee, Y. M.; Garcia, M. A.; Huls, N. A. F.; Sun, S. H. *Angew. Chem., Int. Ed.* **2010**, *49*, 1271.
(24) Metin, O.; Sun, X. L.; Sun, S. H. *Nanoscale* **2013**, *5*, 910.
(25) Li, D. G.; Wang, C.; Tripkovic, D.; Sun, S. H.; Markovic, N. M.; Stamenkovic, V. R. *ACS Catal.* **2012**, *2*, 1358.
(26) Mu, J. B.; Chen, B.; Guo, Z. C.; Zhang, M. Y.; Zhang, Z. Y.; Zhang, P.; Shao, C. L.; Liu, Y. C. *Nanoscale* **2011**, *3*, 5034.
(27) Ravikumar, R.; Gopukumar, S. *Phys. Chem. Chem. Phys.* **2013**, *15*, 3712.
(28) Hansen, H. A.; Varley, J. B.; Peterson, A. A.; Nørskov, J. K. *J. Phys. Chem. Lett.* **2013**, *4*, 388.
(29) Peterson, A. A.; Grabow, L. C.; Brennan, T. P.; Shong, B. G.; Ooi, C. C.; Wu, D. M.; Li, C. W.; Kushwaha, A.; Medford, A. J.; Mbuga, F.; Li, L.; Nørskov, J. K. *Top. Catal.* **2012**, *55*, 1276.
(30) Rodriguez, P.; Koverga, A. A.; Koper, M. T. M. *Angew. Chem., Int. Ed.* **2010**, *49*, 1241.
(31) Lin, C. H.; Chen, C. L.; Wang, J. H. *J. Phys. Chem. C* **2011**, *115*, 18582.
(32) Jiang, T.; Mowbray, D. J.; Dobrin, S.; Falsig, H.; Hvolbaek, B.; Bligaard, T.; Nørskov, J. K. *J. Phys. Chem. C* **2009**, *113*, 10548.
(33) Falsig, H.; Hvolbaek, B.; Kristensen, I. S.; Jiang, T.; Bligaard, T.; Christensen, C. H.; Nørskov, J. K. *Angew. Chem., Int. Ed.* **2008**, *47*, 4835.
(34) Nørskov, J. K.; Rossmeisl, J.; Logadottir, A.; Lindqvist, L.; Kitchin, J. R.; Bligaard, T.; Jonsson, H. *J. Phys. Chem. B* **2004**, *108*, 17886.
(35) Greeley, J.; Jaramillo, T. F.; Bonde, J.; Chorkendorff, I. B.; Nørskov, J. K. *Nat. Mater.* **2006**, *5*, 909.
(36) Qian, H. F.; Zhu, M. Z.; Wu, Z. K.; Jin, R. C. *Acc. Chem. Res.* **2012**, *45*, 1470.
(37) Kleis, J.; Greeley, J.; Romero, N. A.; Morozov, V. A.; Falsig, H.; Larsen, A. H.; Lu, J.; Mortensen, J. J.; Dulak, M.; Thygesen, K. S.; Nøto authorrskov, J. K.; Jacobsen, K. W. *Catal. Lett.* **2011**, *141*, 1067.
(38) Rosen, B. A.; Salehi-Khojin, A.; Thorson, M. R.; Zhu, W.; Whipple, D. T.; Kenis, P. J. A.; Masel, R. I. *Science* **2011**, *334*, 643.